# Plasmonic Field Effects on the Energy Transfer between Poly(p-phenyleneethynylene) Fluorescent Polymer and Au Nanocages

**ARTICLE** *in* THE JOURNAL OF PHYSICAL CHEMISTRY C · JUNE 2011

Impact Factor: 4.77 · DOI: 10.1021/jp2007528



**2 AUTHORS:**

Mahmoud A. Mahmoud
Georgia Institute of Technology
**76** PUBLICATIONS **1,798** CITATIONS
SEE PROFILE

Mostafa A El-Sayed
Georgia Institute of Technology
**675** PUBLICATIONS **54,634** CITATIONS
SEE PROFILE

THE JOURNAL OF PHYSICAL CHEMISTRY C

ARTICLE

pubs.acs.org/JPCC

# Plasmonic Field Effects on the Energy Transfer between Poly(*p*-phenyleneethynylene) Fluorescent Polymer and Au Nanocages

M. A. Mahmoud and M. A. El-Sayed*

Laser Dynamics Laboratory, School of Chemistry and Biochemistry, Georgia Institute of Technology, Atlanta, Georgia 30332-0400, United States

Supporting Information

**ABSTRACT:** Colloidal gold nanocages (AuNCs) with a wall length of 60 nm and wall thickness of 6 nm were prepared by the galvanic replacement method. The AuNCs were assembled into monolayers with different percents of surface coverage, using the Langmuir−Blodgett technique. The same technique was used to coat the assembled monolayers of AuNCs with another monolayer of poly(*p*-phenyleneethynylene) (PPE) fluorescent polymer. The surface plasmon resonance (SPR) spectrum of the AuNCs red-shifts as the percent of AuNCs coverage increases due to growth of the interparticle surface plasmon resonance field coupling as interparticle distance decreases. While after coating the AuNCs array with PPE, the SPR of all the AuNCs monolayers arrays were red-shifted to the same position (693 nm). This unsystematic red-shift behavior is based on the presence of two plasmon fields (inside and outside of AuNCs) and is described by discrete dipole approximation (DDA) simulation. The polymer fluorescence intensity is found to decrease when the polymer is deposited over the AuNCs. This observation is due to the energy transfer between the excited PPE and the AuNCs as well interchain energy transfer. Upon turning on the plasmonic field (exciting the surface plasmon resonance band), it is found that the fluorescence intensity of the polymer increased to a maximum value at AuNCs percent coverage of 10% and then decreased as the interparticle separation distance decreased. DDA calculations showed that this is consistent with the dependence of the SPR field strength on the interparticle separation. Physically, this is a result of the interplay between the changes in the surface plasmon fields within the cavity of each nanoparticle and their external surface fields as a pair of AuNCs approach one another.

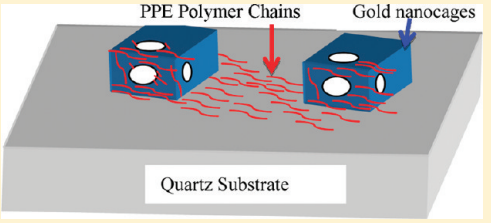


## INTRODUCTION

Plasmonic nanoparticles have been used in many optical[1−3] and biological[4,5] applications. The great versatility of these particles comes from the ability to fine-tune their physical and optical properties.[6−9] When these nanoparticles are irradiated with electromagnetic radiation of the appropriate wavelength, surface plasmon resonance (SPR) of the conduction band electrons takes place and induces strong electromagnetic fields on and around the nanoparticle surface.[6,10,11] SPR of these nanoparticles depends on their shape and size, which is why a wide range of sizes and shapes (spheres,[12] rods,[13] cubes,[14,15] etc.) have been synthesized. The Halas group[16] reported on the tunability of the SPR of gold nanoshells on silica cores and polymer bead cores. The magnitude of the red-shift of the SPR wavelength is found to depend on the ratio of the thickness of the gold nanoshell to the diameter of the entire nanoparticle. The reason for this is discussed in detail in the literature.[17] Similarly, hollow gold nanocages (AuNCs) have attracted great attention because of the tunability of their surface plasmon resonance spectra in the visible and near-IR regions.[18] Many sizes and shapes of AuNCs were synthesized and used in many applications.[15,19,20]

The Langmuir−Blodgett (LB) technique has been used to assemble colloidal nanoparticles prepared by chemical methods.[19,21−23] The advantage of this technique lies in its ability to assemble the nanoparticles into a monolayer at different interparticle separation distances and then deposit monolayers on the surface of the monolayer.[15,19,24,25]

$\pi$-Conjugated fluorescent polymers have strong absorption, emission, and conducting properties, which make them useful in many applications such as electronic devices and sensing.[26−28] When the fluorescent polymer molecules are packed at small distances, rotation of the polymer backbone may become hindered through sterric interactions. This can lead to changes in their emission characteristics[29] due changes in the polymer conformations and interpolymer energy transfer dynamics due to increased probability of energy transfer between chains at short distances. This results in an increased number of diffusion pathways and dynamics of the polymer excitons.[30]

In the present work, using the LB technique, a monolayer of the poly(*p*-phenyleneethynylene) (PPE) fluorescent polymer has been deposited on the top of a monolayer of AuNCs assembled with different surface densities. The position of the SPR band maximum of the AuNCs was measured at different surface pressures in the presence and in the absence of the polymer monolayer. In addition, the fluorescence spectra of PPE were measured in the absence and presence of SPR excitation of

**Received:** January 24, 2011
**Revised:** May 15, 2011
**Published:** May 23, 2011

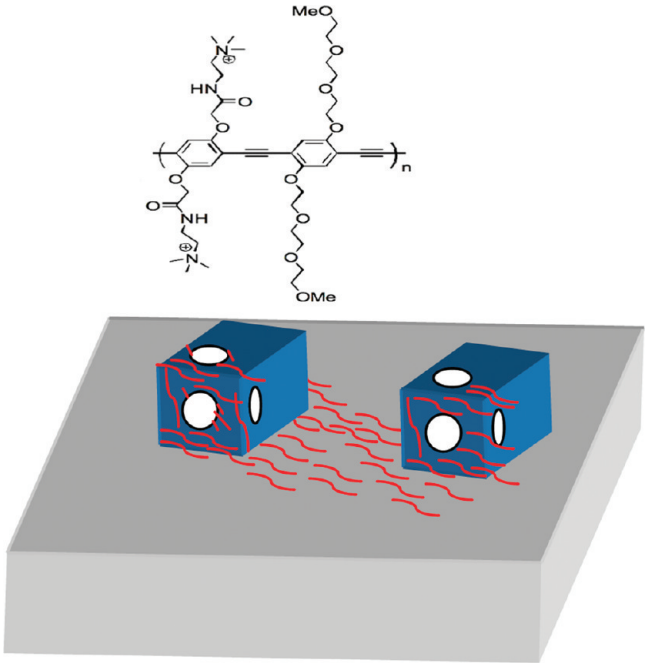


**Figure 1.** Schematic diagram for the different possible arrangements of PPE polymer monolayer deposited on AuNCs monolayer. This arrangement of PPE polymer can be categorized as (1) adsorbed on the top of nanoparticles, (2) anchored inside the nanocages, and (3) sitting in-between the nanoparticles. The red lines represent the PPE polymer chains; the number of polymer units ($n$) is 15 units.

AuNCs. In both cases, the intensity of the fluorescence of the polymer decreases and enhanced upon turning on the nanoparticle surface plasmon field of the AuNCs. The decrease in the fluorescence intensity results is discussed in terms of energy transfer to the ground state of AuNCs as well as to polymer interchains segments and polymer chain−AuNCs interactions. Surface-enhanced Raman spectroscopy (SERS) was used to monitor the arrangement of the PPE around and inside the AuNC hollow nanoparticles.

## EXPERIMENTAL SECTION

Gold nanocages were prepared from the silver nanocubes (AgNCs) by galvanic replacement of silver atoms by gold atoms.[31] The gold atoms built first on the edges of the silver nanocube. Three silver atoms are oxidized by one gold ion. As the amount of gold increase, the size of the AgNCs template shrinks from inside to generate a large cavity within the structure. Silver nanocubes were prepared by heating 35 mL of ethylene glycol (EG) at 150 °C for 1 h, followed by the addition of a solution of 0.3 g of polyvinylpyrrolidone (PVP) (molecular weight of ∼55 000) dissolved in 5 mL of EG. After 5 min, 0.4 mL of sodium sulfide (3 mM) dissolved in EG was added. AgNCs were produced 15 min after adding 0.12 g of $AgNO_3$ dissolved in 5 mL of EG. AgNCs were removed from the EG solvent and excess PVP by dilution with a water−acetone mixture and centrifugation at 13 000 rpm for 5 min. The AgNCs were precipitated down and dispersed in water. Gold nanocages (AuNCs) were prepared by heating AgNCs solution to boiling and then slowly injecting 10 mg/L hydrogen tetrachloroaurate solution until the absorption spectrum of the solution shifted to 810 nm.[32] The AuNC solution was continuously refluxed until the absorption spectrum became stable and then was cleaned as described previously.[33] The AuNCs were moved to chloroform by centrifugation at 10 000 rpm and dispersion in chloroform. The poly($p$-phenyleneethynylene) (PPE) fluorescent polymer, with molecular weight of $1.1 \times 10^4$ g/mol, was prepared as reported earlier (see pages S1−S3 of the Supporting Information).[34]

A Nima 611 D trough was used to assemble the AuNCs into a monolayer at different surface pressures. 0.5 mL of AuNCs in chloroform was sprayed over the surface of the water-filled trough. The surface pressure was monitored with the use of a Wilhelmy plate, attached to a D1L-75 model pressure sensor. Using the same deposition procedure, the PPE dissolved in chloroform was then deposited onto the nanoparticle monolayer at constant surface pressure. Figure 1 shows a schematic diagram illustrating how it is thought that the PPE arrange on the AuNCs monolayer. Absorbance and steady-state fluorescence measurements were taken on an Ocean Optics HR4000Cg-UV-NIR absorption spectrometer and a Horiba Jobin Yvon flourmeter (model FL3-12) with a Hamamatsu photomultiplier tube (R928P), respectively. Scanning electron microscopy (SEM) images were taken using a Zeiss Ultra60 microscope. A Picoscan 5 Molecular Imaging AFM (atomic force microscope) was used for surface profiling.

## RESULTS AND DISCUSSION

**Characterization of AuNCs Monolayers before and after Coating with the PPE Polymer.** *a. SEM and AFM.* As described in the Experimental Section, AuNC monolayers were assembled on the surface of silicon wafer for SEM imaging. Alternatively, the nanoparticles were assembled into a LB monolayer on the surface of quartz substrates for the optical measurements. The AuNCs monolayers assembled on the surface of quartz substrates were further coated with a PPE polymer monolayer. AFM was used to image the surface in order to calculate the thickness of the PPE polymer. The size of the AuNCs was measured from SEM images. The thickness of the PPE monolayer was determined by subtracting the size of the AuNCs, calculated from SEM, from the height of the particles in the 3D AFM image which contain the thicknesses of PPE.

Figure 2A−F shows the SEM images of AuNCs assembled into monolayers by the LB trough at surface pressures of 0, 0.5, 1, 2, 4, and 6 mN/m, respectively. It can be calculated from the SEM images that the particle density increases as the surface pressure, at which the particles were assembled increases. Thus, the interparticle separation distance decreases as the percent coverage increases. With the help of Image-J program, the percent of area coverage is calculated to be 4, 7, 10, 17, 25, and 29% for images in Figure 2A−F, respectively. From the AuNCs synthetic method, AuNCs are capped with PVP polymer. The thickness of the PVP capping material was found to be ∼1 nm. This value is estimated from the distance between two touching side-to-side (dimer) nanoparticles in the SEM image. This distance is constant in all AuNCs monolayer assemblies. This seems logical because all of the samples are prepared from the same monolayer assembled on the LB trough.

AFM is a valuable technique used for 3D imaging topography of material surfaces. The AFM imaging study assisted us in determining the thickness of the PPE polymer monolayer deposited on the surface of the monolayers of AuNCs. Figure 3 shows the AFM images of the 29% surface coverage of AuNC sample after being coated with PPE. Comparison of Figures 2F

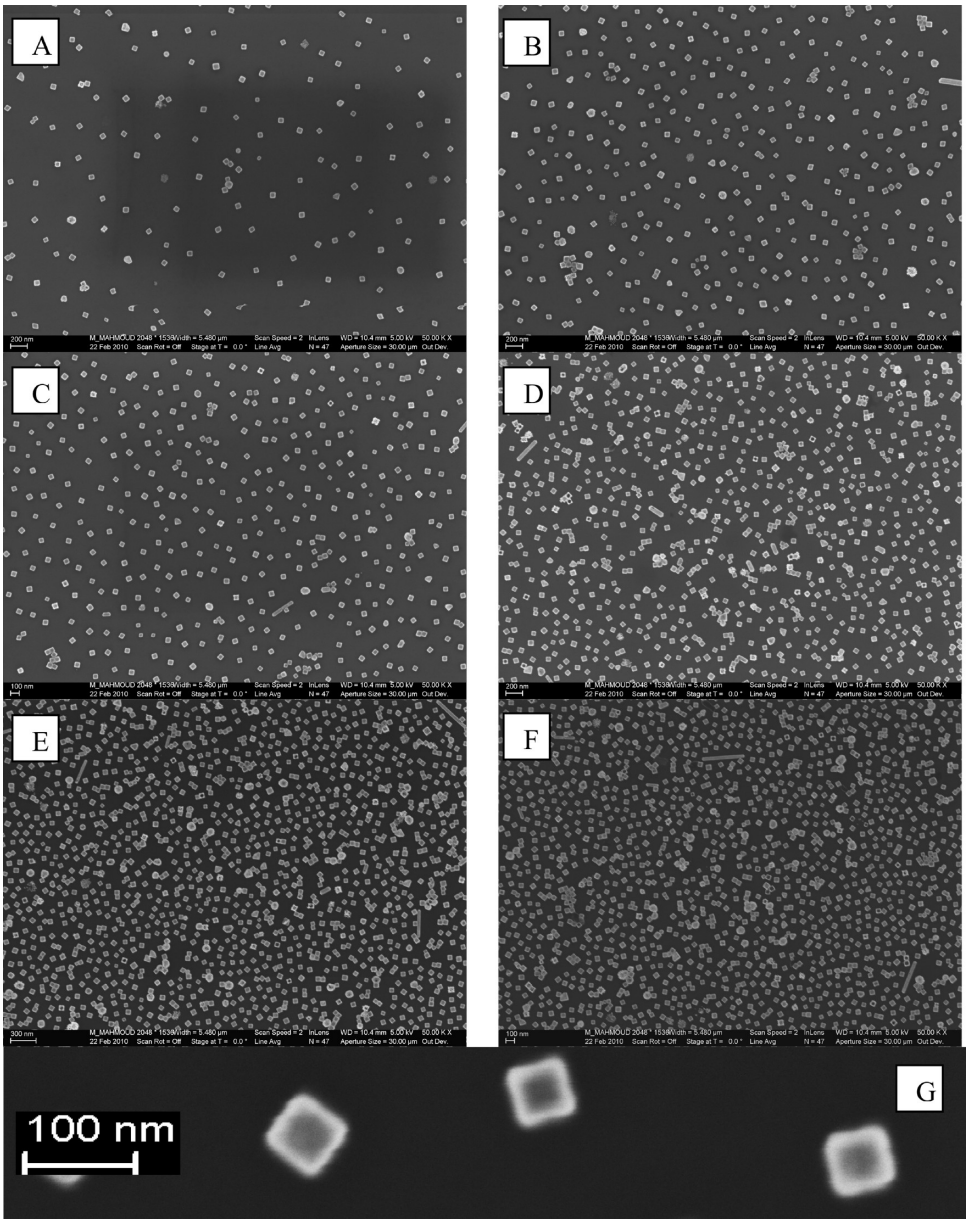


**Figure 2.** (A−F) SEM images of AuNCs monolayers assembled on the surface of silicon wafer at surface pressures of 0, 0.5, 1, 2, 4, and 6 mN/m. (G) Enlarged AuNCs.

and 3A shows that the particle distribution did not change much after polymer coating. The arrangement of the PPE around the AuNCs and on the substrate is uniform (see the 3D AFM in Figure 3B). The thickness of the PPE layer is in the range of 4−5 nm; the space between the particles is not filled with the polymer.

*b. SERS of PPE Polymer Monolayer Deposited on the Top of AuNC Monolayers.* Raman spectroscopy is a valuable technique, providing information about the structural conformations of the functional groups of the analyte.[35] Plasmonic nanoparticles enhance the Raman signal of molecules adsorbed on their surface when the photon of the laser Raman is in resonance with the SPR of the nanoparticles.[36] The relative degree of enhancement, the band shift, and width of the Raman bands depend on the orientation of the molecules on the surface of nanoparticles.[37] Figure 4 shows the polarized SERS spectrum of PPE (parallel and perpendicular modes) which are adsorbed on the surface of AuNCs monolayers assembled at different percent coverage. The SERS spectrum for each sample was compared for parallel and perpendicular polarization modes. The purpose of this measurement is to study the organizations of PPE on the top of AuNCs monolayer assembly. Raman bands appearing at 1506 and 1305 $cm^{-1}$ are assigned as ring stretching vibrations of PPE. In all samples these bands are found to be narrower and sharper in the case of the perpendicular polarization mode as compared to the parallel mode in all samples. Moreover, the band at 1448 $cm^{-1}$, which is assigned as $CH_3$ asymmetric deformation, has the same behavior as the ring stretching modes. While the in-plane CH deformation bands appearing at 1169 and 1123 $cm^{-1}$ showed a small change as the polarization changes, the in-plane ring deformation at 1004 $cm^{-1}$ does not change much. Finally, the out-of-plane ring deformation at 660 $cm^{-1}$ was not changed.

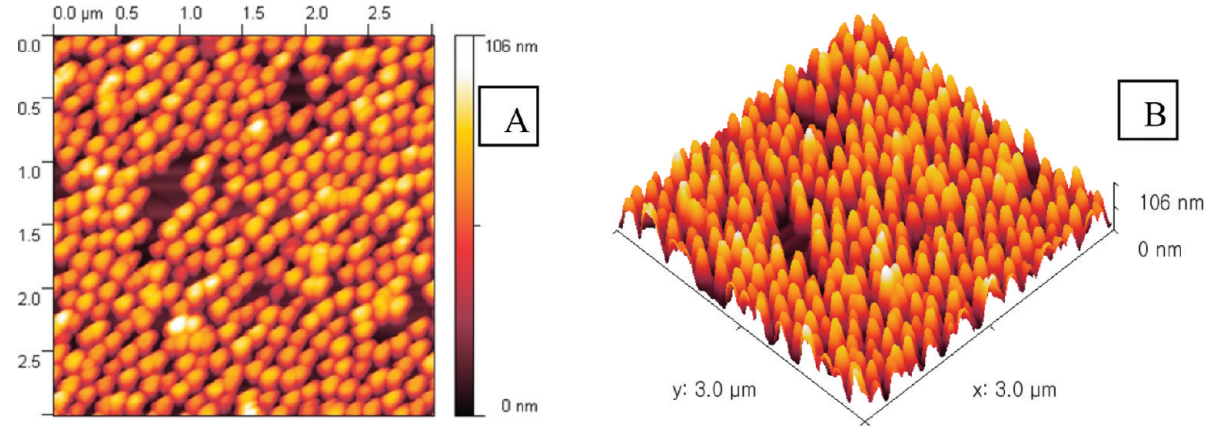


**Figure 3.** AFM image of AuNCs assembled at surface pressure of 6 mN/m (29% coverage) and coated with 4 nm thick monolayer of PPE: (A) 2D view, (B) 3D view.

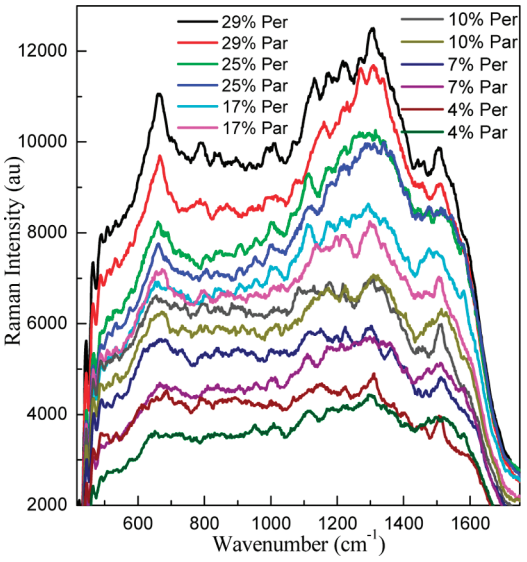


**Figure 4.** SERS of PPE polymer monolayer deposited on the top of AuNC monolayers assembled on the surface of quartz substrate with 4, 7, 10, 17, 25, and 29% surface coverages, for perpendicular (per) and parallel (Par) modes. The changes in the Raman bands are attributed to the changes in the orientations of PPE in and around the AuNCs in the LB monolayer assemblies.

The reason for the different features of SERS spectra for PPE is the organization of the polymer chains with different conformations inside and around the AuNCs. The change in the SERS band shapes supports the schematic diagram in Figure 1 showing the different organization of PPE polymer adsorbed on the top of monolayer AuNCs assemblies.

**Surface Plasmon Resonance Band Maximum Wavelength of AuNCs before and after Coating with PPE Polymer.** The SPR optical peak position of a single nanoparticle depends on its shape and size,[38] while for multiple nanoparticles, it red-shifts by amounts that depends on the interparticle separation.[19] The change in the dielectric constant of the surrounding environment also changes the SPR peak position. The electromagnetic plasmon field accompanying the SPR depends not only on the shape, size, and the interparticle separation (due to the plasmon field coupling) but also on the dielectric function of the medium and the degree of atomic order within the particle (the crystallinity). Polycrystalline nanoparticles lose phase coherence faster than single crystalline materials, which results in broader SPR bandwidth and a lower electromagnetic plasmon field compared to single crystal nanoparticles.[39] The SPR of nanoparticles usually red-shifts with the increase in the particle size.[40] The SPR extinction peak has contribution from absorption and scattering processes. As the particle size increases, the relative contribution of the scattering increases.[41] The SPR peak of hollow gold nanocages shifts to the red as the pore size in their walls increases or their wall thickness decreases.[33]

Figure 5A shows the SPR spectrum of assembled monolayers of gold nanocages with a wall length of 60 nm, deposited on the surface of quartz substrate with different percent coverage. As the interparticle distance decreases by increasing the percent of nanoparticle coverage, the SPR band shifts to the red due to interparticle surface plasmon coupling. For 4% percent coverage, the SPR peak is centered at 675 nm, while for the largest percent coverage (29%), the SPR peak shifts to 691 nm. The other samples have peak positions between 675 and 691 nm. Figure 5B shows the SPR spectra of AuNCs monolayers after being covered with a monolayer of the PPE polymer. In this case the SPR band is observed at 694 nm, independent of the surface coverage. The observed shift from 675 nm for the bare AuNCs is due the increase of the dielectric constant of the PPE polymer medium surrounding the AuNCs. This is different from the observed results reported in our previous study[34] on solid silver nanocube monolayers in which the red-shift in the SPR peak position, after coating with PPE layer, increased as the interparticle separation distances decreased. The reason for dissimilarity in the behavior of solid and hollow nanoparticles is attributed to the presence of one plasmon field inside and one plasmon field outside the nanocage, as will describe in the theoretical calculation section.[33]

The deposition of PPE on the surface of AuNC monolayers was carried out at the same LB surface pressure to make sure that the amounts of the PPE deposited in all samples are similar. Figure 5C is the magnified part of Figure 5B in the absorption region of PPE. It gives the absorption spectrum of the PPE monolayer deposited on the surface of the AuNC monolayer which was assembled at different surface pressures (different percent coverage). The same absorption intensity was observed for all of the PPE samples, either when pure or deposited on the

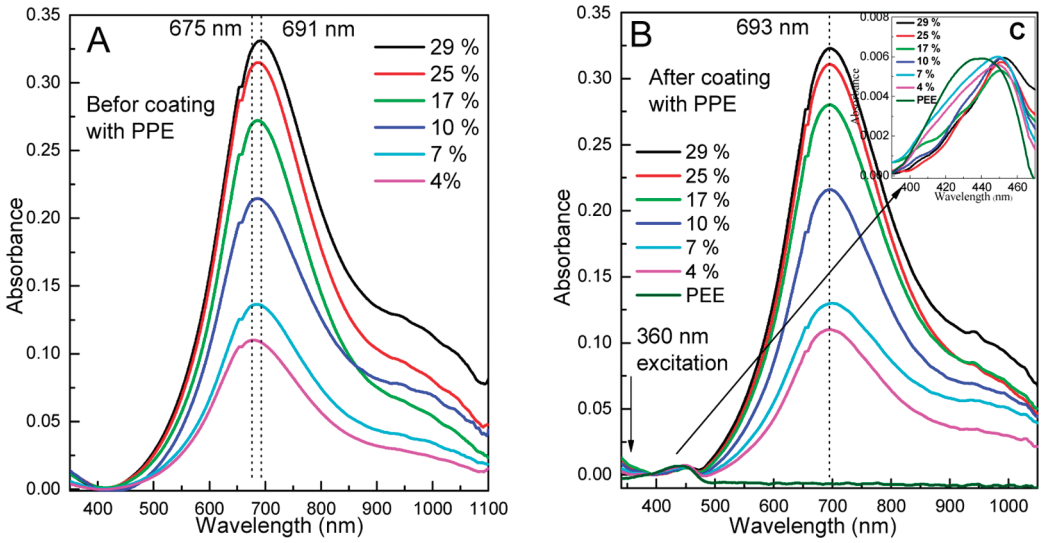


**Figure 5.** (A) Surface plasmon resonance spectra of AuNC monolayers assembled on the surface of a quartz substrate at different percent of covered area. (B) SPR of AuNC monolayer assembled on the surface of quartz substrate after being coated with PPE fluorescent polymer monolayer. (C) Absorption spectra of PPE monolayer deposited on AuNCs monolayer (zoom-in graph B in the range of ~380−470 nm).

AuNCs monolayers, while a red-shift and peak sharpening were observed in the spectra of PPE coating the AuNCs monolayers. In addition to the absorption spectrum of the PPE polymer and the extinction spectrum of AuNCs, the PVP capping the AuNCs has a small absorption contribution at wavelengths shorter than those of the PPE polymer. As a result, the absorption peak intensity of PVP increases slightly as the percent of coverage increases due to the increasing the number of AuNCs particles.

It has been reported that bends or twists of the chains of the $\pi$-conjugated polymers result in the formation of different conformations which break the $\pi$-conjugation[42] to varying extents. These changes in the conformations of the conjugated polymers produce chromophores with a wide range of conjugation lengths. Because the excitation energy depends strongly on the conjugation length, the polymer displays an inhomogeneous distribution of absorption energies. The large observed variation in the band shapes of the absorption spectra of PPE on the top of AuNCs monolayers[30] in Figure 4C can result from this as well as from the different intermolecular interactions energies in a disordered solid PPE. Indeed, the AuNCs take part in the organization of PPE polymer chains (see Figure 4C). The reason for the red-shift in the absorption spectra of PPE coating AuNCs could be attributed either to a charge transfer interaction between the PPE and the AuNCs or to increasing the average conjugation length of the polymer chains.[43,44]

**Plasmonic Field Effect on the Steady-State Fluorescence.** *a. Polymer Fluorescence Intensity in the Polymer−AuNC Monolayers in the Absence of Plasmonic Excitation.* The optical measurement of AuNCs coated with monolayer of PPE polymer, as shown in Figure 5B, has three extinction peaks: the first peak is the absorption spectrum peak of PVP that is capping the AuNCs during the synthesis, the second peak corresponds to the absorption spectrum of PPE fluorescence polymer, and the third is the SPR spectrum of the AuNCs which is centered at 693 nm. When the AuNCs−PPE samples are exposed to a photon with energy of 360 nm, only PVP capping polymer and PPE fluorescence polymer will be excited. PPE fluoresces and its fluorescence spectrum overlaps with the SPR of the AuNCs, while PVP does not. Figure 6A shows the fluorescence spectrum of the PPE polymer monolayer which has been deposited over AuNCs monolayer with different percent of coverage. The general observation is that the fluorescence intensity of PPE polymer does not change regardless of the percent coverage. Moreover, the intensity of the fluorescence spectrum in the case of pure PPE monolayer is found to be 5 times higher than that of the PPE−AuNCs system.

The absorption intensity of PVP, as shown in Figure 5B, increases as the percent of coverage increases. We expect the PVP to absorb more photons as the percent of coverage increases, but in fact the fluorescence spectrum of the PPE polymer does not change as the percent of coverage AuNCs increases and so the PVP capping polymer does not transfer its excitation energy to the PPE polymer.

PPE is a cationic-conjugated semiconducting fluorescent polymer.[34] The interaction of the PPE with the unexcited nanoparticles is found to change the fluorescence intensity. It has been reported that fluorescence quenching is observed when the SPR peak overlaps with the emission band.[45] The quenching could result from one of the three possible mechanisms. The first mechanism could involve energy or electron transfer processes. In the Förster resonance energy transfer mechanism, the quenching rate depends on the overlap between the fluorescence and the SPR bands. By using plasmonic nanoparticles with different SPR peak wavelength positions, one is able to change such overlap and thus the quenching efficiency. In the gold nanosphere−PPV polymer, it was found that the quenching efficiency was independent of the overlap, suggesting an electron transfer mechanism.[46,47] The second mechanism could be static quenching resulting from the columbic interaction between the plasmonic nanoparticles and the charge on the PPE.[46] The third mechanism could be long-range energy transfer within the conjugated polymer chains.[46]

It has been reported that the quenching efficiency of the fluorescence depends on the distance between the nanoparticles and fluorescent materials.[48] This is why the distance between the nanoparticles and the PPE fluorescence polymer is kept constant

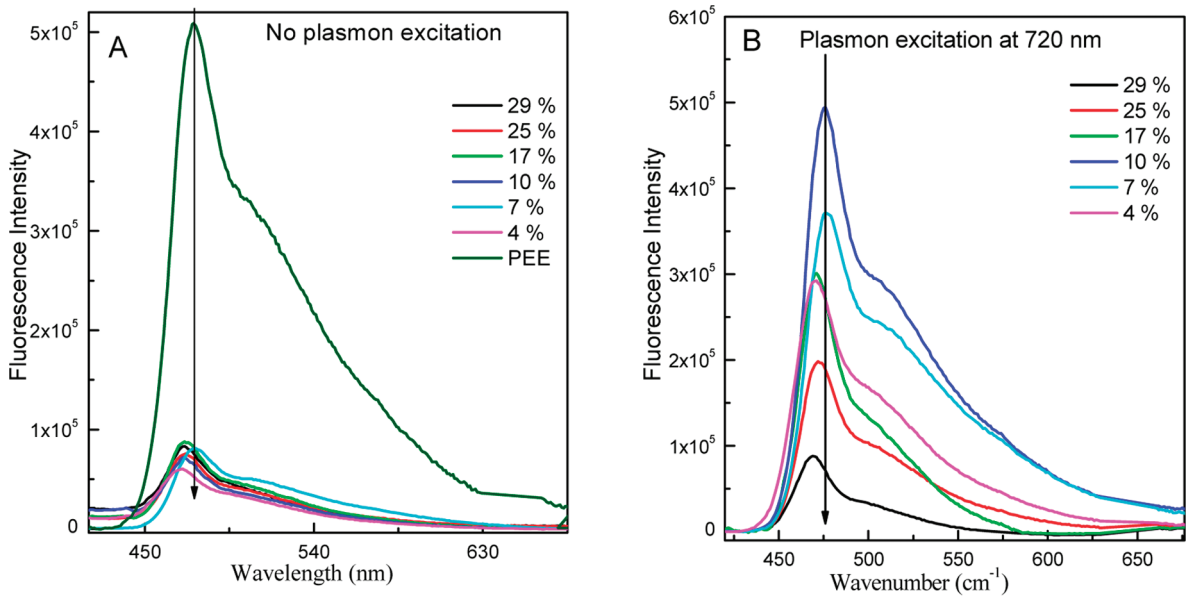


**Figure 6.** Steady-state fluorescence spectra of PPE polymer deposited on the top of AuNC monolayers assembled at percent of coverage area of 4, 7, 10, 17, 25, and 29%, resulting from excitation at 360 nm photon: (A) without exciting the plasmon of AuNCs; (B) with exciting the plasmon at 720 nm.

in the present work (since the aim of this work is to monitor the effect of turning on the plasmon field of AuNCs on the fluorescence quenching of PPE). From SEM and AFM images, the thickness of the PVP capping material layer around the AuNCs was calculated and found to be thinner than ~1 nm.

Previous theoretical modeling studies had shown that the interchain effects in the $\pi$-conjugated fluorescent polymer are important only in close-packed polymer systems.[49] Time-resolved studies on the $\pi$-conjugated polymers had established that energy can be transferred rapidly between polymer segments with different conjugation lengths[50−54] or between polymer segments and other chromophores[55−58] via Förster type transfer[59,60](dipole−dipole coupling) mechanism. The transfer time is a few picoseconds,[50,51,54,55,59] which is much shorter than the emission lifetime. The emission is thus usually observed only from the longest conjugated polymer that has the lowest energy.[34] Therefore, for our PPE−AuNCs system there are two factors affecting the observed polymer fluorescence intensity. The first is the composition of the polymer segments that have different conjugation length. The second is the percent of coverage of nanoparticles. As the degree of ordering of PPE polymer increases (system with fewer conformations), the average conjugation length increases and the amount of quenching of the high-energy emission increases. From Figure 5C, the degree of ordering of the PPE chains increases and the absorption red-shifts as the percent coverage of AuNCs increases.

The average length of PPE polymer (estimated by ChemBio 3D Ultra, assuming a linear configuration) would be ~20 nm. As shown in Figure 1, the organization of PPE monolayers over AuNCs monolayer is divided into three categories: (1) adsorbed on the top of nanoparticles, (2) anchored inside the nanocages, and (3) located as a monolayer in-between the nanoparticles. The quenching of the fluorescence of the PPE molecules located in-between the nanoparticles is affected mainly by the interchain energy transfer and degree of conjugation, while the adsorbed polymer on the outer surface of the nanoparticles is quenched by the energy or electron transfer between the PPE and the nanoparticles as well as the polymer interchain self-quenching. Finally, the quenching of the fluorescence of the PPE anchored inside the nanoparticles is affected by both the interchain energy transfer (polymer self-quenching) and the polymer−particles energy transfer. When the AuNCs percent of coverage increases, the effect on the emission of the polymer chains anchored inside the AuNCs at the expense of the amount of polymer located between the AuNCs determine what is observed (due to the increase in the number of nanoparticles). Therefore, quenching due to PPE−AuNCs energy transfer is more dominant, while the interchain quenching becomes dominant when the percent coverage decreases. For this reason, the quenching of PPE fluorescence has the same amount in the case of all the samples regardless of the percent of surface coverage by AuNCs. The observed red-shift in the fluorescence results from the interchain interactions and polymer−particle interaction because the exciting energy levels are lowered when the exciton becomes increasingly delocalized.[43,44]

*b. Polymer Fluorescence Intensity of the Polymer-Excited AuNC System; Plasmonic Field Effects.* Figure 5A shows the fluorescence spectrum of PPE when excited at 360 nm. This excitation wavelength does not excite the SPR of AuNCs. Figure 6B shows the steady-state fluorescence of PPE monolayers deposited on AuNC monolayer when excited at 360 and 720 nm simultaneously. It is observed that the intensity of the fluorescence spectra of PPE in the presence of the plasmon field increases as the percent of coverage increases until it reaches a maximum value at 10% coverage and then decreases. In fact, the intensity of the fluorescence of pure PPE polymer is more intense than the PPE polymer on AuNCs. From Figure 6A,B the quenching in the fluorescence spectra is observed if the plasmon of the AuNC is excited or not. The degree of quenching is much greater when the SPR is not excited compared to when SPR is excited. Figure 7 shows the fluorescence intensity of PPE coating the AuNCs monolayers and the intensity of fluorescence in the pure PPE monolayer as a function of percent of surface coverage when the plasmon field is and is not excited. When the plasmon

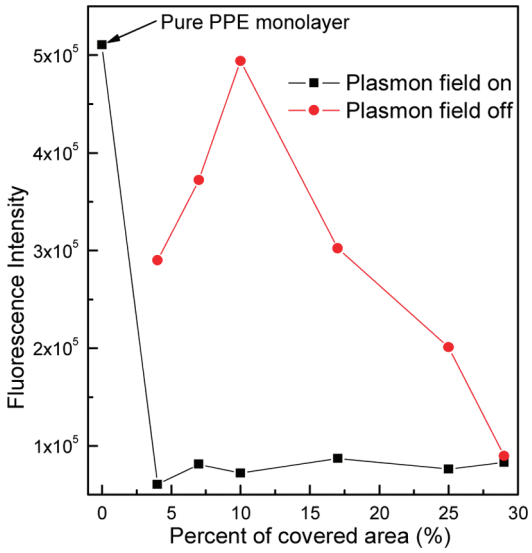


**Figure 7.** Fluorescence intensity of PPE coating AuNCs assembled at different percent of covered area: (black curve) when the plasmon is not excited, the fluorescence intensity is almost constant as the percent of covered area increase; (red curve) when the plasmon field is excited by 720 nm photon, the fluorescence increases as the percent of covered area increases until 10% coverage and then decreases as the percent of covered area by the AuNCs increases.

field is not excited, the fluorescence intensity does not change much as the percent of coverage increases. When the SPR of the AuNCs is excited, the fluorescence increases to a maximum value at 10% AuNCs coverage and decreases afterward. This suggests that the fluorescence intensity increases as the coverage increases when the plasmon field is on until the percent coverage reaches 10% and decreases afterward.

**DDA Calculations and the Plasmonic Field Effect on the Fluorescence Intensity of AuNCs.** In order to explain Figure 7 showing the increase and subsequent decrease in the PPE polymer fluorescence intensity, plasmonic field intensity is calculated as a function of the interparticle distance of the nanoparticle in a dimer. Two theoretical models are commonly used to simulate the absorption, scattering, and the plasmon field enhancement factor of the plasmonic nanoparticles[61] (i.e., discrete dipole approximation (DDA)[62] and the finite difference time domain (FTDA)[63]). Here we used the DDA simulation method to calculate the plasmon field enhancement factor as well as the SPR.[62] For solid shaped plasmonic nanoparticles, the plasmon field for the single nanoparticle is stronger than a pair of nanoparticle, and the density of this plasmon field is usually highest in the region between the nanoparticle pairs.[64,65] In order to understand the reason for the shift in the SPR spectra of AuNCs monolayers (with different percent of coverage) to the same SPR spectrum peak position after coating with PPE, the DDA calculations were carried out. However, the field enhancement factor was calculated for a pair of AuNCs fixed at different distances. Figure 7A−D shows the electromagnetic field enhancement factor map contour of a pair of AuNC with wall length of 60 nm, wall thickness of 6 nm, and a 12 × 12 nm hole in each wall (mimicking the experimentally prepared particles as shown in Figure 2). Unlike the solid plasmonic nanoparticles, the AuNCs pair placed at a separation of 6 nm has a weak electromagnetic plasmon field in-between the two nanocages (coupling zone) as compared to the field at the far corners.[66] When these AuNCs pairs are placed at a 12 nm separation, the electromagnetic field in-between the two nanocages increases but is still less than the plasmon field intensity at the far corners. When the nanocages pair is fixed at separation distance of 60 nm, the field intensity between the AuNC pairs is increased compared to the pairs placed at smaller separations. At a larger separation between the AuNC pairs (180 nm), the field intensity in both the area between the nanoparticles and the corners becomes comparable. The field intensity in the AuNCs holes was found to decrease as the interparticle separation distance of the nanoparticles pair decreases until the distance becomes 30 nm. After this point, the field intensity increases again, and the maximum value was observed at 180 nm separations as shown in Figure 8E.

The above calculations can be summarized as follows: As the interparticle separation distance increases, the field outside the AuNCs decreases while the field at the AuNCs holes increases. It is well established that as the dielectric constant of the surrounding medium increases, the SPR peak position red-shifts and the amount of red-shift is correlated to the intensity of the electromagnetic field.[67] On the basis of the DDA calculation results and the SEM images, we can describe the unexpected red-shift in the SPR spectrum peak positions to the same wavelength (683 nm) after coating the AuNC monolayer with a PPE layer. Although before coating, a red-shift was observed to increase with the increasing percent of surface coverage (see Figure 4). AuNCs have two surfaces: outer and inner surfaces. The outer surface is coated with PVP capping material, and the inner surface is slightly clean. This means that the inner surface is more sensitive to the change in the dielectric constant value of the added chemical (PPE) than the outer surface, and the red-shift in the SPR peak position depends greatly on the plasmonic field on the inner surface. For samples with high AuNCs surface coverage, most of the nanoparticles are set at small interparticle separation distance, and so the plasmon field inside is weak. As a consequence, the shift in the SPR peak position is small as the dielectric constant increases by replacing air with PPE polymer. For samples with low AuNCs percent of coverage, the majority of nanoparticles have large interparticle separation distance and so the plasmon field inside AuNCs becomes high, and a great red-shift in the SPR peak position was observed as the dielectric constant increases.

The plasmon field enhancement calculations can be used to describe the plasmon field effect on the fluorescence intensity. However, as shown in Figure 5, the fluorescence spectrum of PPE coating the AuNCs monolayer assembly (while exciting the AuNC SPR at 720 nm) has a different behavior compared to the fluorescence spectra measured in the absence of AuNCs SPR excitation. When the AuNCs are excited, the induced localized surface plasmon resonance of the nanoparticle generated a strong electromagnetic field at the surface of the nanoparticle. The electromagnetic field could enhance the polymer fluorescence intensity, especially the PPE in-between the AuNCs. Furthermore, the fact that the nanoparticles are excited decrease the efficiency of the energy transfer (and thus the quenching) between the excited polymers and the nonexcited nanoparticles.

As mentioned earlier, PPE has different arrangements on the AuNCs monolayer assemblies (e.g., they could be located between the nanoparticles, adsorbed on the surface of the particles, or anchored inside the pores of the nanoparticles). For the PPE adsorbed on the surface of AuNCs or anchored inside their pores, the PPE−AuNCs energy transfer decreases

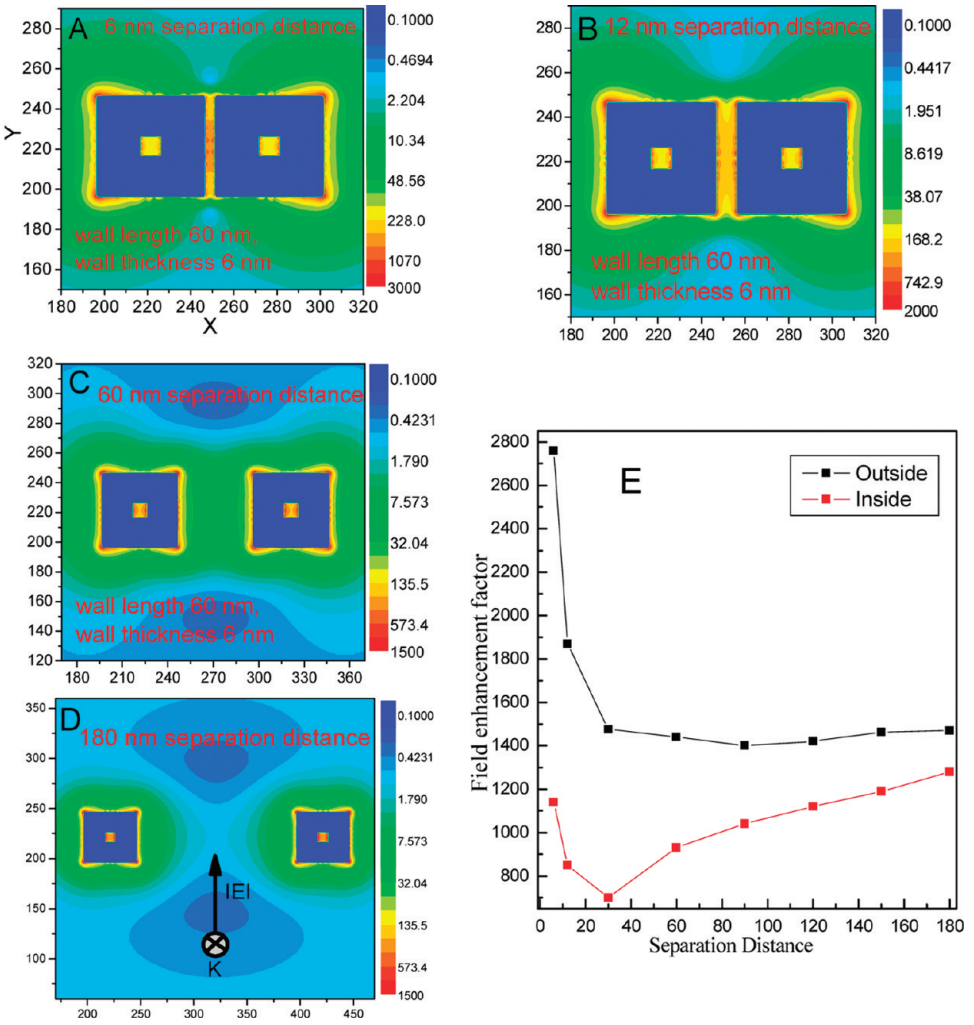


**Figure 8.** Electromagnetic field enhancement contour maps on the outside surface of AuNC pairs with wall thickness of 6 nm and placed at different separation distance: panels A, B, C, and D are 6, 12, 60, and 180 nm, respectively. (E) Relationship between the plasmon fields (black) outside and (red) inside the holes and the interparticle separation distance of a pair of AuNCs.

after the AuNCs SPR excitation. This occurs because the electrons of AuNCs will be in the excited state, and this hinders the delivery of the excitation energy of PPE by AuNCs. Therefore, as the AuNCs percent of coverage increases, the amount of surface adsorbed and pores anchored with PPE polymer increases and the percent of PPE fluorescence quenching decreases. This is why the intensity of fluorescence for PPE in all samples after excitation of the SPR is more intense compared to the absence of SPR excitation. If the energy transfer is the only effective mechanism, the relationship between the percent of coverage and fluorescence should be linear, but what was observed is that fluorescence intensity increases until 10% coverage and then decreases afterward. The major reason for this behavior is that the quenching effect of the plasmon field for the fluorescence of PPE sitting in-between the AuNCs takes place by the dipole−dipole coupling (Förster mechanism). The field outside the AuNCs is only playing a role in the quenching effect of the PPE sitting in-between the AuNCs; as the plasmon field outside the AuNCs becomes stronger, the quenching efficiency increases.

According to DDA calculations, the electromagnetic field enhancement of a pair of AuNCs, placed at different separation distances, decreases as the interparticle separation distance decreases until the distance reaches 30 nm. Below this distance the field intensity increases. In comparison, for the experimental and the plasmon field calculations at high percent of coverage, most of the nanoparticles are present at a small separation distance, at which the plasmon field is strong and the amount of fluorescence quenching of the PPE located in-between the AuNCs is high; when the percent of coverage decreases, the majority of the nanoparticles are at larger distance as in the case of 10% coverage, so the plasmon field decreases and hence the rate of fluorescence quenching decreases (as in the case of plasmon field calculations at 30 nm separation distance). Ultimately, when the percent of coverage decreases, the majority of the nanoparticles becomes at large separation area (more than 30 nm) and the plasmon field becomes stronger. This is why the rate of quenching increases again by decreasing the percent of coverage area below 30%. For the samples with percent of coverage of 4 and 7%, the distance between the nanoparticles is large enough so the interchain quenching is also efficient. This supports what is shown in Figure 6; the fluorescence decreases as the percent of surface coverage of AuNCs increases more than 10% coverage, and as the percent of coverage increases, the percent of quenching increases.

## ■ ASSOCIATED CONTENT

**Supporting Information.** Synthesis procedure of PPE fluorescence polymer (pages S1−S3); electromagnetic field enhancement contour maps on the inside surface of AuNC pairs with wall thickness of 6 nm and placed at different separation distance (page S4). This material is available free of charge via the Internet at http://pubs.acs.org.

## ■ AUTHOR INFORMATION

**Corresponding Author**
*E-mail: melsayed@gatech.edu.

## ■ ACKNOWLEDGMENT

This work was supported by the Department of Energy Grant DE-FG02-09ER46604. We thank A. Poncheri and R. Phillips for proofreading the manuscript and providing us with PPE polymer.

## ■ REFERENCES

(1) Phillips, R. L.; Miranda, O. R.; You, C. C.; Rotello, V. M.; Bunz, U. H. F. *Angew. Chem., Int. Ed.* **2008**, *47*, 2590.
(2) Haes, A. J.; Chang, L.; Klein, W. L.; Van Duyne, R. P. *J. Am. Chem. Soc.* **2005**, *127*, 2264.
(3) Berger, C. E. H.; Beumer, T. A. M.; Kooyman, R. P. H.; Greve, J. *Anal. Chem.* **1998**, *70*, 703.
(4) Urbina, M. C.; Zinoveva, S.; Miller, T.; Sabliov, C. M.; Monroe, W. T.; Kumar, C. *J. Phys. Chem. C* **2008**, *112*, 11102.
(5) Ghosh, P. S.; Kim, C. K.; Han, G.; Forbes, N. S.; Rotello, V. M. *ACS Nano* **2008**, *2*, 2213.
(6) Link, S.; El-Sayed, M. A. *Int. Rev. Phys. Chem.* **2000**, *19*, 409.
(7) Jain, P. K.; Huang, X. H.; El-Sayed, I. H.; El-Sayed, M. A. *Acc. Chem. Res.* **2008**, *41*, 1578.
(8) Grzelczak, M.; Perez-Juste, J.; Mulvaney, P.; Liz-Marzan, L. M. *Chem. Soc. Rev.* **2008**, *37*, 1783.
(9) Perez-Juste, J.; Pastoriza-Santos, I.; Liz-Marzan, L. M.; Mulvaney, P.; Elsevier Science: Amsterdam, **2005**; *Coord Chem. Rev.* **2005**, *249*, 1870−1901.
(10) Kerker, M. *J. Colloid Interface Sci.* **1985**, *105*, 297.
(11) Creighton, J. A.; Eadon, D. G. *J. Chem. Soc., Faraday Trans.* **1991**, *87*, 3881.
(12) Freund, P. L.; Spiro, M. *J. Phys. Chem.* **1985**, *89*, 1074.
(13) Nikoobakht, B.; El-Sayed, M. A. *Chem. Mater.* **2003**, *15*, 1957.
(14) Sun, Y. G.; Xia, Y. N. *Science* **2002**, *298*, 2176.
(15) Mahmoud, M. A.; El-Sayed, M. A. *J. Phys. Chem. C* **2008**, *112*, 14618.
(16) Oldenburg, S. J.; Averitt, R. D.; Westcott, S. L.; Halas, N. J. *Chem. Phys. Lett.* **1998**, *288*, 243.
(17) Wang, H.; Brandl, D. W.; Nordlander, P.; Halas, N. J. *Acc. Chem. Res.* **2007**, *40*, 53.
(18) Skrabalak, S. E.; Au, L.; Li, X.; Xia, Y. *Nature Protoc.* **2007**, *2*, 2182.
(19) Mahmoud, M. A.; El-Sayed, M. A. *Nano Lett.* **2009**, *9*, 3025.
(20) Hu, M.; Chen, J.; Li, Z.-Y.; Au, L.; Hartland, G. V.; Li, X.; Marquez, M.; Xia, Y. *Chem. Soc. Rev.* **2006**, *35*, 1084.
(21) Tao, A.; Kim, F.; Hess, C.; Goldberger, J.; He, R. R.; Sun, Y. G.; Xia, Y. N.; Yang, P. D. *Nano Lett.* **2003**, *3*, 1229.
(22) Tao, A.; Sinsermsuksakul, P.; Yang, P. *Nature Nanotechnol.* **2007**, *2*, 435.
(23) Huang, J. X.; Kim, F.; Tao, A. R.; Connor, S.; Yang, P. D. *Nature Mater.* **2005**, *4*, 896.
(24) Mahmoud, M. A.; Snyder, B.; El-Sayed, M. A. *J. Phys. Chem. C* **2011**ASAP.
(25) Mahmoud, M. A.; Tabor, C. E.; El-Sayed, M. A. *J. Phys. Chem. C* **2009**, *113*, 5493.
(26) Bunz, U. H. F. *Acc. Chem. Res.* **2001**, *34*, 998.
(27) Feng, F. D.; He, F.; An, L. L.; Wang, S.; Li, Y. H.; Zhu, D. B. *Adv. Mater.* **2008**, *20*, 2959.
(28) McQuade, D. T.; Pullen, A. E.; Swager, T. M. *Chem. Rev.* **2000**, *100*, 2537.
(29) Bunz, U. H. F.; Imhof, J. M.; Bly, R. K.; Bangcuyo, C. G.; Rozanski, L.; Bout, D. A. V. *Macromolecules* **2005**, *38*, 5892.
(30) Nguyen, T.-Q.; Doan, V.; Schwartz, B. J. *J. Chem. Phys.* **1999**, *110*, 4068.
(31) Chen, J.; Wiley, B.; Li, Z.-Y.; Campbell, D.; Saeki, F.; Cang, H.; Au, L.; Lee, J.; Li, X.; Xia, Y. *Adv. Mater. (Weinheim, Ger.)* **2005**, *17*, 2255.
(32) Yen, C. W.; Mahmoud, M. A.; El-Sayed, M. A. *J. Phys. Chem. A* **2009**, *113*, 4340.
(33) Mahmoud, M. A.; Snyder, B.; El-Sayed, M. A. *J. Phys. Chem. C* **2010**, *114*, 7436.
(34) Mahmoud, M. A.; Poncheri, A. J.; Phillips, R. L.; El-Sayed, M. A. *J. Am. Chem. Soc.* **2010**, *132*, 2633.
(35) Nakamoto, K. *Infrared and Raman Spectra of Inorganic and Coordination Compounds. Part A: Theory and Applications in Inorganic Chemistry*, 5th ed.; Wiley-Interscience: New York, 1997.
(36) Moskovits, M. *J. Chem. Phys.* **1978**, *69*, 4159.
(37) Badr, Y.; Mahmoud, M. A. *J. Mol. Struct.* **2005**, *749*, 187.
(38) Kreibig, U.; Vollmer, M. *Optical Properties of Metal Clusters*; Springer Series in Materials Science 25; Springer: Berlin, 1995.
(39) Ziegler, T.; Hendrich, C.; Hubenthal, F.; Vartanyan, T.; Trager, F. *Chem. Phys. Lett.* **2004**, *386*, 319.
(40) Tabor, C.; Murali, R.; Mahmoud, M.; El-Sayed, M. A. *J. Phys. Chem. A* **2009**, *113*, 1946.
(41) Lee, K.-S.; El-Sayed, M. A. *J. Phys. Chem. B* **2006**, *110*, 19220.
(42) Nguyen, T.-Q.; Wu, J.; Doan, V.; Schwartz, B. J.; Tolbert, S. H. *Science (Washington, D. C.)* **2000**, *288*, 652.
(43) Nguyen, T.-Q.; Martini, I. B.; Liu, J.; Schwartz, B. J. *J. Phys. Chem. B* **2000**, *104*, 237.
(44) Nguyen, T.-Q.; Kwong, R. C.; Thompson, M. E.; Schwartz, B. J. *Appl. Phys. Lett.* **2000**, *76*, 2454.
(45) Fan, C.; Wang, S.; Hong Janice, W.; Bazan Guillermo, C.; Plaxco Kevin, W.; Heeger Alan, J. *Proc. Natl. Acad. Sci. U. S. A.* **2003**, *100*, 6297.
(46) Fan, C.; Wang, S.; Hong, J. W.; Bazan, G. C.; Plaxco, K. W.; Heeger, A. J. *Proc. Natl. Acad. Sci. U. S. A.* **2003**, *100*, 6297.
(47) Swager, T. M. *Acc. Chem. Res.* **1998**, *31*, 201.
(48) Dulkeith, E.; Ringler, M.; Klar, T. A.; Feldmann, J.; Javier, A. M.; Parak, W. J. *Nano Lett.* **2005**, *5*, 585.
(49) Ruini, A.; Caldas, M. J.; Bussi, G.; Molinari, E. *Phys. Rev. Lett.* **2002**, *88*, 206403/1.
(50) Kersting, R.; Lemmer, U.; Mahrt, R. F.; Leo, K.; Kurz, H.; Baessler, H.; Goebel, E. O. *Phys. Rev. Lett.* **1993**, *70*, 3820.
(51) Lemmer, U.; Mahrt, R. F.; Wada, Y.; Greiner, A.; Baessler, H.; Goebel, E. O. *Chem. Phys. Lett.* **1993**, *209*, 243.
(52) Hayes, G. R.; Samuel, I. D. W.; Phillips, R. T. *Phys. Rev. B: Condens. Matter* **1995**, *52*, R11569.
(53) Kersting, R.; Mollay, B.; Rusch, M.; Wenisch, J.; Warmuth, C.; Kauffmann, H. F. *J. Lumin.* **1997**, *72*−*74*, 936.
(54) Warmuth, C.; Tortschanoff, A.; Brunner, K.; Mollay, B.; Kauffmann, H. F. *J. Lumin.* **1998**, *76&77*, 498.
(55) Haring Bolivar, P.; Wegmann, G.; Kersting, R.; Deussen, M.; Lemmer, U.; Mahrt, R. F.; Baessler, H.; Goebel, E. O.; Kurz, H. *Chem. Phys. Lett.* **1995**, *245*, 534.
(56) Dogariu, A.; Gupta, R.; Heeger, A. J.; Wang, H. *Synth. Met.* **1999**, *100*, 95.
(57) Cerullo, G.; Graupner, W.; Lanzani, G.; Nisoli, M.; List, E. J. W.; Stagira, S.; De Silvestri, S.; Leising, G. *Synth. Met.* **1999**, *101*, 306.
(58) Wohlgenannt, M.; Graupner, W.; Wenzl, F. P.; Tasch, S.; List, E. J. W.; Leising, G.; Graupner, M.; Hermetter, A.; Rohr, U.; Schlichting, P.; Geerts, Y.; Scherf, U.; Mullen, K. *Chem. Phys.* **1998**, *227*, 99.
(59) Kersting, R.; Mollay, B.; Rusch, M.; Wenisch, J.; Leising, G.; Kauffmann, H. F. *J. Chem. Phys.* **1997**, *106*, 2850.

(60) Förster, T. *Ann. Phys.* **1948**, *2*, 55−75.
(61) Mahmoud, M. A.; Snyder, B.; El-Sayed, M. A. *J. Phys. Chem. Lett.* **2010**, *1*, 28.
(62) Draine Bruce, T.; Flatau Piotr, J. *J. Opt. Soc. Am. A* **2008**, *25*, 2693.
(63) Sherry, L. J.; Chang, S.-H.; Schatz, G. C.; Van Duyne, R. P.; Wiley, B. J.; Xia, Y. *Nano Lett.* **2005**, *5*, 2034.
(64) Haes, A. J.; Haynes, C. L.; McFarland, A. D.; Schatz, G. C.; van Duyne, R. P.; Zou, S. *MRS Bull.* **2005**, *30*, 368.
(65) Haes, A. J.; Zou, S.; Schatz, G. C.; Van Duyne, R. P. *J. Phys. Chem. B* **2004**, *108*, 6961.
(66) Sherry, L. J.; Jin, R.; Mirkin, C. A.; Schatz, G. C.; Van Duyne, R. P. *Nano Lett.* **2006**, *6*, 2060.
(67) Mahmoud, M. A.; El-Sayed, M. A. *J. Am. Chem. Soc.* **2010**, *132*, 12704.